THE EUROPEAN
PHYSICAL JOURNAL A

Pairing correlations within the micro-macroscopic approach for the level density

A. G. Magner[1,2,a] [ORCID], **A. I. Sanzhur**[1], **S. N. Fedotkin**[1], **A. I. Levon**[1], **U. V. Grygoriev**[1,3], **S. Shlomo**[2]

[1] Institute for Nuclear Research, Kyiv 03028, Ukraine
[2] Cyclotron Institute, Texas A&M University, College Station, TX 77843, USA
[3] University of Groningen, 9712 TS Groningen, The Netherlands

Communicated by David Blaschke

Abstract Level density $\rho(E, N, Z)$ is calculated for the two-component close- and open-shell nuclei with a given energy E, and neutron N and proton Z numbers, taking into account pairing effects within the microscopic-macroscopic approach (MMA). These analytical calculations have been carried out by using semiclassical statistical mean-field approximations beyond the saddle-point method of the Fermi gas model in a low excitation-energies range. The level density ρ, obtained as function of the system entropy S, depends essentially on the condensation energy $E_{\rm cond}$ through the excitation energy U in super-fluid nuclei. The simplest super-fluid approach, based on the BCS theory, accounts for a smooth temperature dependence of the pairing gap Δ due to particle number fluctuations. Taking into account the pairing effects in magic or semi-magic nuclei, excited below neutron resonances, one finds a notable pairing phase transition. Pairing correlations sometimes improve significantly the comparison with experimental data.

1 Introduction

Many properties of heavy nuclei can be described in terms of the level density [1–16]. In close relation to the statistical level density [4,6], this article is devoted to the memory of Professor Peter Schuck, in particular, to his fruitful ideas of the semiclassical pairing treatment in nuclear physics and associated areas [17–32]. The level density $\rho(E, N, Z)$, where E, N and Z are the energy, neutron and proton numbers, respectively, is given by the inverse Laplace transformation of the partition function $\mathcal{Z}(\beta, \boldsymbol{\alpha})$ [1]. Within the grand canonical ensemble, the standard saddle-point method (SPM) is used for integration over all Lagrangian multipliers, β for the energy E and $\boldsymbol{\alpha} = \{\alpha_n, \alpha_p\}$ for neutron N and proton Z numbers [1,2]. This method assumes large excitation energies U, so that the temperature T is related to a well-determined saddle point β^* in the integration variable β for a finite Fermi system of large neutron and proton numbers in a nucleus, $T = 1/\beta^*$. However, data from many experiments for energy levels and spins also exist for low excitation energy U, where such a saddle point does not exist. Moreover, there is a pairing effect which can be extremely important at low U. For presentation of experimental data on low-energy nuclear spectra, the cumulative level-density distribution – cumulative number of quantum levels below the excitation energy U – is conveniently often calculated for statistical analysis of the experimental data on collective excitations [33]. Therefore, to simplify the calculations of the level density, $\rho(E, N, Z)$, we carry out [34–39] the integration over the Lagrange multiplier β in the inverse Laplace transformation of the partition function $\mathcal{Z}(\beta, \boldsymbol{\alpha})$ analytically but more accurately beyond the SPM for small and large shell-structure contributions [40]. Thus, for the integration over β we will use approximately the micro-canonical ensemble which does not assume a temperature and an existence of thermodynamic equilibrium.

For formulation of the unified microscopic canonical and macroscopic grand-canonical approximation (MMA) to the level density [34–39], we found a simple analytical approximation for the level density ρ which satisfies the two well-known limits. One of them is the Fermi gas asymptote, $\rho \propto \exp(S)$ for large entropy S [1]. Another limit is the combinatoric expansion in powers of S for a small entropy S or excitation energy U; see Refs. [1,41].

In the calculation of level density at low excitation energies in nuclei, we will consider the system of inter-

a e-mail: magner@kinr.kiev.ua (corresponding author)

acting Fermi particles with a macroscopic number $A = N + Z$, described by the Hamiltonian of the well-known nuclear super-fluid model [42,43], taking mainly the simplest Bardeen-Cooper-Schrieffer (BCS) [44] theory of superconductivity [5,14,18,45]. This method was used also in the level density calculations [4,6] for the description of the superfluidity properties of nuclei, and for other problems such as in nuclear astrophysics; see, e.g., Ref. [46]. We should emphasize the well-known self-consistent method of superfluidity calculations, the Hartree-Fock-Bogoliubov (HFB) theory [18]. Within a mean field approximation, as BCS or HFB approaches, the pairing gap Δ depends sharply on the excitation energy U in the phase transition from a super-fluid to a normal nuclear state. However, as shown in Ref. [19], if we take into account also the particle number fluctuations by using the projected HFB approach, the gap Δ becomes a smooth function of temperature T, in contrast to any mean field models. Smooth behavior of the pairing gap has been found also and carefully studied by analytical methods associated with the extended Thomas-Fermi (ETF) approach, see Refs. [17,20–24,26]. Therefore, we cannot use the normalstate properties of the shell closure, in particular, for magic nuclei like ^{40}Ca, ^{48}Ca, ^{56}Ni, and ^{208}Pb, to deduce that the pairing transition from a super-fluidity to the normal state does not exist there. Our present work was partially initiated also by the recent experimental studies in Ref. [47] in order to clarify their relation to the super-fluidity in magic nuclei. Pairing correlation can in fact influences the level density in magic nuclei, and the question is what are other reasons for difficulty in its experimental observation in magic nuclei, see Refs. [18,39]. This question cannot be separated from the study of the shell structure effects in magic nuclei. Thus, the qualitative study of reasons for a super-fluidity in magic nuclei is one of the main purposes under consideration in this work.

For a deeper understanding of the correspondence between the classical and the quantum approach and simplifying the problem for analytical derivations, it is worthwhile to analyze the shell and pairing effects in the statistically averaged level density ρ, see Refs. [4,6,34], by using the semiclassical periodic-orbit (PO) theory (POT) [48–51]. We extended the MMA approach [34] in Refs. [35–39], for semiclassical description of the shell and isotopic asymmetry effects in the level density of complex nuclei. Smooth properties of the level density as function of the nucleon number A have been studied within the framework of self-consistent ETF approach [7,13,52]. However, for instance, the pairing effects in the statistical MMA level density ρ are still attractive subjects [4,6,14,15,40]. See also common ideas and a very intensive recent analytical study of pairing effects within the semiclassical Wigner-Kirkwood $\hbar$ expansion including nuclear surface $\hbar^2$ corrections; see Refs. [29,32] and references therein.

Table 1 Acronyms and their content

Abbreviations	Content
SPM	Saddle-point method
MMA	Micro-macroscopic approach
BCS	Bardeen-Cooper-Schrieffer
HFB	Hartree-Fock-Bogoliubov
ETF	Extended Thomas-Fermi
POT	Periodic-orbit theory
LES	Low energy states
FG	Fermi gas
LMSF	Least mean-square fits
ENSDF	Evaluated nuclear structure data file
SCM	Shell correction method
s.p.	single-particle

In the present paper, we will present the expressions of MMA for the level density $\rho(E, N, Z)$ in Section 2. The basic formulation of pairing contributions to the MMA level density is shown in Section 3. Section 4 is devoted to the discussion of the results. Summary of the work and perspectives are discussed in Section 5. Some details for the semiclassical periodic orbit theory are given in Appendix A.

2 Microscopic-macroscopic approach

For the statistical description of level density ρ of a nucleus in terms of the total energy, E, and the neutron, N, and proton, Z, numbers, one can begin with the micro-canonical expression [1,2]:

$$\rho(E, N, Z) = \int \frac{\mathrm{d}\beta \mathrm{d}\boldsymbol{\alpha}}{(2\pi i)^3} \exp[S(\beta, \boldsymbol{\alpha})], \qquad (1)$$

where $S = \ln \mathcal{Z}(\beta, \boldsymbol{\alpha}) + \beta E - \boldsymbol{\alpha}\mathbf{N}$, and $\mathbf{N} = \{N, Z\}$ with the total particle number $A = N + Z$. The partition function $\mathcal{Z}$ depends on the Lagrange multipliers, β and $\boldsymbol{\alpha} = \{\alpha_n, \alpha_p\} = \beta\boldsymbol{\lambda}$. The neutron and proton chemical potential components are given by $\boldsymbol{\lambda} = \{\lambda_n, \lambda_p\}$, where $\lambda_n = \alpha_n/\beta$ and $\lambda_p = \alpha_p/\beta$. The entropy $S(\beta, \boldsymbol{\alpha})$ can be expanded in power series over $\boldsymbol{\alpha}$ for a given β near the saddle point $\boldsymbol{\alpha}^*$,

$$S(\beta, \boldsymbol{\alpha}) = S(\beta, \boldsymbol{\alpha}^*) + (1/2)\left(\partial^2 S/\partial \boldsymbol{\alpha}^2\right)^* \left(\boldsymbol{\alpha} - \boldsymbol{\alpha}^*\right)^2 + \dots . \qquad (2)$$

The Lagrange multiplier, $\boldsymbol{\alpha}^*$, and the chemical potential $\boldsymbol{\lambda}$, are defined in terms of the neutron and proton relatively large particle numbers $\mathbf{N}$ by a saddle-point condition,

$$\left(\frac{\partial S}{\partial \boldsymbol{\alpha}}\right)_{\alpha=\alpha^*} \equiv \left(\frac{\partial \ln \mathcal{Z}}{\partial \boldsymbol{\alpha}}\right)_{\alpha=\alpha^*} - \mathbf{N} = 0 . \qquad (3)$$

In order to avoid the SPM divergences for the zero excitation energy limit (Table 1), we will integrate over β in Eq. (1) more accurately using the statistically averaged excitation energy U as a measure of the mean nuclear excitations, instead of the temperature T. Integrating over α in Eq. (1) by the standard SPM, using the expansion (2), one obtains

$$\rho(E, N, Z) \approx \frac{1}{4\pi^2 i} \int d\beta \, \beta \mathcal{J}^{-1/2} \exp\left(\beta U + a/\beta\right) , \quad (4)$$

where $U = E - E_0$ is the excitation energy and E_0 is the total neutron and proton energy background, and a is the level density parameter. In Eq. (4), $\mathcal{J}$ is the Jacobian,

$$\mathcal{J} = \mathcal{J}\left(\frac{\partial \Omega}{\partial \lambda_n}, \frac{\partial \Omega}{\partial \lambda_p}; \lambda_n, \lambda_p\right)^* = \left(\frac{\partial^2 \Omega}{\partial \lambda_n^2} \frac{\partial^2 \Omega}{\partial \lambda_p^2}\right)^*, \quad (5)$$

where Ω is the thermodynamic potential,

$$\Omega = \ln \mathcal{Z}/\beta . \quad (6)$$

The asterisk in Eq. (5) indicates the saddle point, Eq. (3), for the integration over α at any β. We assumed here that the neutron, λ_n, and proton, λ_p, chemical potentials are close to a mean value λ, and similarly, $a_n \approx a_p \approx a/2$ for the level density parameter. Then, as shown in Refs. [35,36] (including the shell effects), for sufficiently low energies, U, the Jacobian $\mathcal{J}$, and the exponent in Eq. (4) mainly have a simple β dependence. Indeed, the thermodynamic potential Ω, Eq. (5), under such small excitation energies takes a simple form:

$$\Omega \approx \Omega_0 - \frac{a}{\beta^2} , \quad \Omega_0 = E_0 - \lambda A , \quad (7)$$

where Ω_0 is the thermodynamical potential background. To reduce the integral over β in Eq. (4) to the textbooks Laplace transforms, we use the approximate and rather accurate evaluation of the integrand factor, $\mathcal{J}^{-1/2}$, where $\mathcal{J}$ is the Jacobian, Eq. (5). According to Eqs. (5) and (7), the Jacobian, $\mathcal{J}^{1/2}$, can be written as

$$\mathcal{J} \approx (1/4) E_0''^2 (1 + \xi) , \quad \xi = -2a''/(\beta^2 \Omega_0''), \quad (8)$$

where the primes denote derivatives of the level density parameter, $a(\lambda)$, and background part of the thermodynamic potential, $\Omega_0(\lambda)$, Eq. (7), and $E_0(\lambda)$, over the mean chemical potential λ. The expression (8) for ξ can be evaluated approximately at the saddle point $\beta \sim \beta^* = 1/T = (a/U)^{1/2}$ in the integration over β, Eq. (4), $\xi \sim \xi^*$. This estimate can be used to simplify the Jacobian factor $\mathcal{J}^{1/2}$ in the integrand of Eq. (4). It is convenient to relate the value ξ^* to the energy shell corrections δE by using the POT expression, Eq. (A5); see Appendix A and Refs. [48,50],

$$\xi^* = -\frac{2a''}{\beta^{*2}\Omega_0''} \approx \frac{8\pi^6 U A^{1/3}}{3a\lambda^2} \mathcal{E}_{sh} ,$$
$$\mathcal{E}_{sh} = -\frac{\delta E}{E_{ETF}} A . \quad (9)$$

Table 2 The Bessel function index ν (second column), the coefficients $\overline{\rho}_\nu$ (third column) in the basic formula, Eq. (10), for the level density ρ_{MMA}, short notations (fourth column) for different MMA approaches (1st column); ξ^* is given by Eq. (9), $\kappa = (\pi^2 a''/3a)^{1/2}$

Approach	ν	$\overline{\rho}_\nu$	notations	Criterion
MMA1	2	$2\pi a/3$	(i)	$\xi^* \ll 1$
MMA2a	3	$4\pi a^2/(3\kappa)$	(ii)	$\xi^* \gg 1$
MMA2b	3	$2\sqrt{6}\,\lambda a^2/3$	(ii)	$\xi^* \gg 1$

Here, β^* is the saddle-point value of β mentioned above, and E_{ETF} is the ETF energy component, $E_{ETF} \approx (1/2)\lambda^2 g_{ETF}$, and $g_{ETF} \sim g_{TF} = 3A/2\lambda$. We took into account the factor 4 for the proton-neutron degeneracy. The energy shell correction, δE, can be approximated, for a major shell structure, within the semiclassical POT accuracy, by Eq. (A4) (see Refs. [35,36,39,48,50,51]). In derivations of Eq. (9) we used that any derivative of a in Eq. (7) for the Jacobian $\mathcal{J}$, Eq. (5), leads to the appearance of multiplier of the order of $\mathbb{S}/\hbar \sim A^{1/3}$, where $\mathbb{S}$ is the classical action for the leading periodic orbit; see Appendix A, Eq. (A7). The characteristic parameter ξ^*, Eq. (9), proportional to $\mathcal{E}_{sh}$, specifies the two different approximations, $\xi^* \ll 1$ and $\xi^* \gg 1$, for small and large shell correction contribution $\mathcal{E}_{sh}$, respectively (see Table 2). We will consider below mainly nuclei, for which one has the case of relatively large $\mathcal{E}_{sh}$ and, therefore, large ξ^*.

Thus, expanding the Jacobian factor, $\mathcal{J}^{1/2}$ with Eq. (8), over ξ for small ξ (i) and large ξ (ii) (see fourth column in Table 2) in the integrand over β [Eq. (4)], one takes the standard inverse-Laplace integrals. The convergence in these expansions over ξ was studied in Ref. [36]. Finally, one arrives at the following analytical expressions for the level density $\rho(E, N, Z)$; see Refs. [35,36]:

$$\rho \approx \rho_{MMA}(S) = \overline{\rho}_\nu S^{-\nu} I_\nu(S) , \quad S = 2\sqrt{aU} . \quad (10)$$

Here, $I_\nu(S)$ is the modified Bessel function of the entropy S, which depends on the excitation energy U through the entropy S. The latter will account for the pairing effects in the next section. In this function, one has the index $\nu = 3$ (ii) for the shell structure dominance and $\nu = 2$ (i) for small shell contributions as shown in Table 2. The coefficients $\overline{\rho}_\nu$ are also given in Table 2. In Eq. (10), the value of ν depends on the number of the integrals of motion beyond the energy E and of the shell structure contribution, which is determined by Eq. (9) for ξ^* (see Table 2).

As shown in Table 2 (Ref. [35]), one thus finds, Eq. (10), that $\nu = 2$ and $\overline{\rho}_2 \propto a$ for small ξ^*, named as MMA1 (i) approach while $\nu = 3$ and $\overline{\rho}_3$ for large ξ^*, for the MMA2 approach. Within the MMA2 approach, one may also use a full analytical approach for small values of shell corrections but with large shell contributions due to their significant

derivatives; see general MMA2a approach and its approximation MMA2b in Table 2. The reason for MMA2b approach is large derivatives of the grand-canonical potential Ω, Eq. (7) over the chemical potential λ, as shown above with the help of Appendix A. This is in contrast to the MMA2a approach with evaluations of the $\mathcal{E}_{\text{sh}}$ by using the numerical results of Ref. [53].

Notice that the Fermi-gas (FG) asymptotes [35] can be obtained by using the full SPM approach [1] at $\xi^* \to 0$,

$$\rho_{\text{FG}}(E, N, Z) = \frac{\sqrt{\pi} \exp(2\sqrt{aU})}{12 a^{1/4} U^{5/4}} . \tag{11}$$

As seen and well known, they are divergent at $U \to 0$, in contrast to the finite results of Eq. (10).

3 Pairing effects

Following Refs. [4,6], one can reduce the level density calculation for the system of interacting Fermi-particles described by the two-body Hamiltonian to that of the system of a mean field with the quasi-particles Hamiltonian [5,18]. For neutrons (protons) one writes

$$\hat{H} - \lambda \hat{N} = \sum_{js} (\varepsilon_j - \lambda) \, \hat{a}_{js}^+ \hat{a}_{js} - G \sum_{jj'} \hat{a}_{j+}^+ \hat{a}_{j-}^+ \hat{a}_{j'-} \hat{a}_{j'+} . \tag{12}$$

Here, ε_j is the single-particle energy of states j, which are doubly degenerated over the spin projection sign, $s = \pm$, and $\lambda \approx \lambda_n \approx \lambda_p$ is the chemical potential. For the operator of the total particle number, $\hat{N}$, one has $\hat{N} = \sum_{js} \hat{a}_{js}^+ \hat{a}_{js}$. In Eq. (12), a_{js}^+ and a_{js} are the operators of the creation and annihilation of particles, respectively; see details in Refs. [4,6]. The second term in Eq. (12) is the pairing interaction with the constant G ($G \approx G_n \approx G_p$), which is the averaged matrix element of the residue interaction. The pairing gap Δ is determined by the corresponding equation [18]:

$$\Delta = \frac{G}{2} \sum_j \frac{\Delta}{\sqrt{(\varepsilon_j - \lambda)^2 + \Delta^2}} . \tag{13}$$

In this case one has a very simple and powerful model for the description of the pairing properties of nuclei. The interaction constant G (neutron G_n and proton G_p) can be determined using experimental data [2,6]. The corresponding thermodynamic average of any operator $\hat{Q}$ is determined by

$$\langle \hat{Q} \rangle = \text{Tr} \left[\hat{Q} \exp(-\beta H) \right] / \text{Tr} \left[\exp(-\beta H) \right] . \tag{14}$$

Up to a constant, the Hamiltonian H, Eq. (12), coincides with that of the Fermi quasi-particles in a mean field. Therefore, for the entropy S, one can use the similar expression:

$$S = 2 \sum_j \left[\beta \epsilon_j \bar{n}_j - \ln(1 - \bar{n}_j) \right], \tag{15}$$

where $\epsilon_j = [(\varepsilon_j - \lambda)^2 + \Delta^2]^{1/2}$, and $\bar{n}_j = [1 + \exp(\beta \epsilon_j)]^{-1}$ are the quasi-particle energies, and occupation numbers averages, respectively [4]. In particular, one can find [45] the critical value of the temperature T_c for disappearance of pairing correlations. Introducing, for convenience, the potential, Eq. (7) in the mean field approach, one has to specify the system through the Hamiltonian taking into account the pairing correlations within the simplest approach based on the BCS theory [18,44,45].

Straightforward analytical derivations [4–6,45] valid near the critical point of the superfluid-normal phase transition lead to the critical temperature T_c,

$$T_c = e^C \Delta / \pi , \tag{16}$$

where $C \approx 0.577$ is the Euler constant.

For a given temperature T, when exists, by minimization of the expectation value for the grand-canonical potential Ω, one has (see Refs. [4,6]),

$$\Omega \equiv E - \lambda \mathbf{N} - S/\beta = \langle \hat{H} - \lambda \hat{N} - \hat{S}/\beta \rangle , \tag{17}$$

where $\langle ... \rangle$ denotes a statistical average over the operator enclosed in angle brackets. Here, $\hat{N}$ is the particle (neutron and proton) number and $\hat{S}$ is the entropy operators. For the pairing ground-state energy $\langle H_0 \rangle$, which equals $\langle H \rangle$ at zero excitation energy, $U = 0$, one finds $\langle H_0 \rangle \approx \Delta^2/4G$. With the heat part, $U_c = a T_c^2$ [with Eq. (16) for T_c], where a is the level density parameter, one obtains for the total excitation energy U_c^{tot} of the mean superfluid-collapse transition,

$$U_c^{\text{tot}} = a T_c^2 + \Delta^2/(4G) . \tag{18}$$

The statistically averaged condensation energy E_{cond} can be derived in simple form in terms of the constant pairing gap Δ, independent of the quasi-particle spectrum [2,18,46]. For constant Δ, one can use its averaged empiric dependence on the particle number A, $\Delta \approx 12 A^{-1/2}$ MeV [2,4,6,18]. The results for the level density are weakly dependent on the variation (within 15%) of the number in front of $A^{-1/2}$, also when we replace this power dependence by that suggested in Ref. [54]. This phenomenological behavior $\Delta(A)$ is good for sufficiently heavy nuclei, in particular, for $A \gtrsim 40$.

For the entropy S in Eq. (10), one finds

$$S \approx S_{\text{eff}} = 2\sqrt{a U_{\text{eff}}} , \tag{19}$$

where U_{eff} is the excitation energy, shifted due to the pairing correlations,

$$U_{\text{eff}} = U - E_{\text{cond}} \geq 0 . \tag{20}$$

For the condensation energy E_{cond}, one finally has [4,6, 18]

$$E_{\text{cond}} = \frac{3a\Delta^2}{2\pi^2} \approx \frac{216}{\pi^2 K} \text{ MeV}, \tag{21}$$

where $K = A/a$ is the inverse level density parameter. For $K \sim 10 - 30$ MeV [13,35,36], one obtains $E_{\mathrm{cond}} \approx 1 - 2$ MeV. Notice also that, the condensation energy E_{cond}, Eq. (21), depends on the particle number A mainly through the inverse level density parameter K for $\Delta = 12/A^{1/2}$ MeV. This parameter depends on A [35,36] is basically due to shell effects. For small and large $S = S_{\mathrm{eff}}$, one obtains from the general equation (10) the well-known combinatoric [41] and Fermi gas [1] asymptotes using the important S^2 and $1/S$ corrections, respectively,

$$\frac{\rho_{\mathrm{MMA}}(S)}{\overline{\rho}_\nu} \rightarrow \frac{2^{-\nu}}{\Gamma(\nu+1)} \left[1 + \frac{S^2}{4(\nu+1)} + \mathcal{O}(S^4)\right], \quad S \ll 1,$$

$$\frac{\rho_{\mathrm{MMA}}(S)}{\overline{\rho}_\nu} \rightarrow \frac{\exp(S)}{S^\nu \sqrt{2\pi} S} \left[1 - \frac{1-4\nu^2}{8S} + \mathcal{O}\left(\frac{1}{S^2}\right)\right], \quad S \gg 1, \quad (22)$$

where Γ is the gamma function.

4 Discussion

In Figs. 1 (Table 3) and 2 (Table 4) we present results of theoretical calculations of the statistical level density $\rho(E, N, Z)$ (in logarithms) within the MMA approach, Eq. (10), and its FG limit, Eq. (11), as functions of the excitation energy U for different nuclei.

In Fig. 1, these results are compared with the experimental data for the close-shell magic nuclei ^{40}Ca (a) and ^{56}Ni (b), semi-magic nucleus ^{54}Fe (c) and open-shell non-magic nucleus ^{52}Fe (d), accounting for pairing contributions. Pairing effects in ^{56}Ni and ^{52}Fe nuclei are studied experimentally in details in Ref. [47]. In Fig. 2 we display the results for other nuclei ^{48}Ca, ^{115}Sn, ^{144}Sm, and ^{208}Pb. Our results are obtained by using the values of the inverse level density parameter K, found from their one-parametric least mean-square fits (LMSF) of the MMA results to the experimental data [55]. The data shown by dots with error bars in Figs. 1 and 2 are obtained for the statistical level density $\rho(E, N, Z)$ from the experimental ENSDF [55] data on the excitation energies U and spins I of the quantum states spectra by using the sample method, $\rho_i = L_i/U_s$, where L_i is the number of states in the ith sample, $i = 1, 2, ..., \aleph$ [3,6,36]. The dots are plotted at mean-weighted positions U_i of the excitation energies for each ith sample. Convergence of the sample method over the equivalent sample-length parameter U_s of the statistical averaging was studied under the statistical plateau condition over the K values. The lengths U_s (or the equivalent number of samples $\aleph$) play a role which is similar to that of averaging parameters in the Strutinsky smoothing procedure for the shell correction method (SCM) calculations of the averaged single-particle level density [40]. The plateau condition in our calculations means the almost constant value of the physical parameter K (with better than 20% accuracy) within a relatively large change of sample numbers $\aleph$. Therefore, the

results of Tables 3 and 4, calculated at the same values of the found plateau, do not depend, with the statistical accuracy, on the averaging parameter $\aleph$ within the plateau. The *statistical condition, $L_i \gg 1$,* at different plateau values $\aleph$ determines the accuracy of our statistical calculations. As in the SCM, in our calculations within the sample method with good plateau values for the sample numbers, $\aleph$, shown in the caption of Fig. 1, one obtains a relatively smooth statistical level density as function of the excitation energy U. We require such a smooth behavior because the statistical fluctuations of particle numbers are neglected in our theoretical derivations of the level density.

The relative error σ of the standard LMSF (see Tables 3 and 4), for the description of the spectra data, in terms of the statistically averaged level density ρ_i, is given by the standard formula through the χ^2 of the LMSF, $\sigma^2 = \chi^2/(\aleph - 1)$ is the relative error dispersion. The error σ determines the applicability of the theoretical approximations, $\rho(U_i)$. These experimental results are practically independent of the model. One of the important reason is that we use the plateau condition over the number of points $\aleph$. This is similar to that of the SCM (Ref. [40]) but in contrast to many other presentations; cf., e.g. with Refs. [10,11]. We do not use empiric (non-physical) free fitting parameters. We discuss the level density $\rho(E, N, Z)$ integrated over spins accounting for degeneracy over their projections. In particular, this $\rho(E, N, Z)$ is independent of assumptions for using the approximation of small spins, and there is no explicit dependence of ρ on the nuclear moment of inertia.

Figure 1 shows the results for four different situations concerning pairing contributions. In the upper plots of Fig. 1 we present two magic nuclei with the red pairing-collapse arrow far away on right of the 1st experimental data point for ^{40}Ca (a), and slightly on its left for ^{56}Ni (b), respectively. In both panels, one has a significant excitation-energy gap below the first data point in close-shell magic nuclei. In contrast to them, in the lower plots Fig. 1c and d we show a semi-magic and non-magic examples for the nuclei ^{54}Fe and ^{52}Fe, respectively, where the first experimental point appears at a relatively small excitation energy U. The super-fluid collapse (red arrow) is placed in Fig. 1c, d on a finite distance from the first excited state, which is of the order of the condensation energy E_{cond}.

Thus, we do not expect significant pairing effects for the nucleus ^{56}Ni (Fig. 1b and Table 3) which agrees with experimental studies in Ref. [47]. However, it is related to the superfluid-normal phase transition itself, rather than to a shell closure in nucleus ^{56}Ni in its normal state. Best conditions for the experimental observation of a super-fluidity transition in studied nuclei can be found, in our opinion, in ^{40}Ca, see Fig. 1a and Table 3 because of the sufficiently large distance in the positive direction between the first excited state and estimated arrow for U_c^{tot}, Eq. (18), for the pairing collapse. It
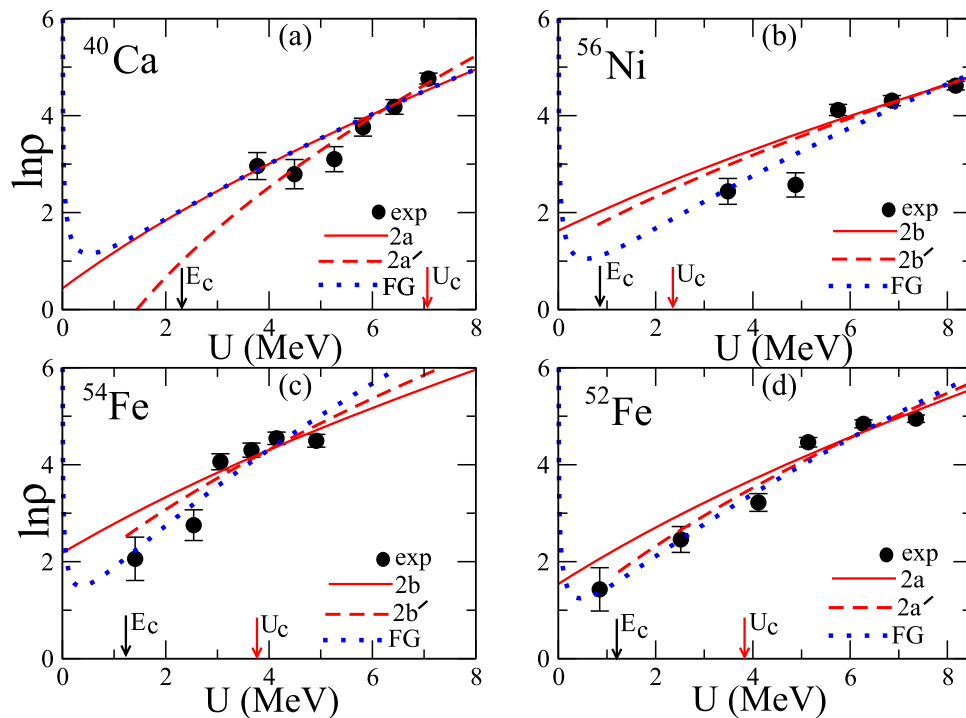
Fig. 1 Level density, $\ln\rho(E, N, Z)$, for low energy states in the magic (close-shell) ^{40}Ca (a) and ^{56}Ni (b), semi-magic ^{54}Fe (c) and non-magic (open-shell) ^{52}Fe (d) nuclei. Solid lines show the results of the MMA for the minimal value of the least mean square (LMS) error σ, Eq. (10), Table 3, by neglecting the pairing condensation. Dashed lines are the same but taking into account the pairing effect through the condensation energy E_{cond} [Table 3, Eq. (21)]. Blue dotted lines present the Fermi gas (FG) approach [1]. The chemical potential is $\lambda = 40$ MeV. Exper-imental close circles are obtained directly from the excitation energy data [55] by using the sample method [35,36]. The plateau condition was checked within the number of dots $\aleph = 5 - 8$ over the inverse level density parameter K. Black ($E_c = E_{cond}$), and red ($U_c = U_c^{tot}$) arrows present the evaluations of the condensation energy (21), and the excita-tion energy (18) for the phase superfluid-normal transition, respectively

Table 3 The inverse level density parameter K (sixth column) and its error (seventh column), found by the LMSF with relative accuracy σ (eighth column), for the nuclei shown in the first column (see Fig. 1)

Nuclei	MMA	$\mathcal{E}_{sh}$	E_{cond} (MeV)	U_c^{tot} (MeV)	K (MeV)	ΔK (MeV)	σ
^{40}Ca	2a′	0.061	2.3	7.1	9.6	0.3	1.3
	2a				12.5	0.3	1.6
	FG				13.4	0.4	1.5
^{56}Ni	2b′	0.008	0.80	2.50	27.3	0.7	2.2
	2b				29.0	0.7	2.4
	FG				17.8	0.7	3.2
^{54}Fe	2b′	0.264	1.23	3.82	17.9	0.8	1.9
	2b				21.1	0.7	1.9
	FG				12.5	0.5	2.3
^{52}Fe	2a′	0.003	1.23	3.84	17.7	0.5	2.5
	2a				20.1	0.5	2.4
	FG				15.4	0.5	2.7

The second column displays the MMA method: MMA2a′ or MMA2b′ with the finite condensation energy E_{cond}, and MMA2a or MMA2b with no pairing, and all versus FG model. The relative shell (with pairing) corrections $\mathcal{E}_{sh}$, Eq. (9) (from Ref. [53]), are shown in the third column. The fourth and fifth columns show the found condensation energies E_{cond}, Eq. (21), and total excitation energies U_c^{tot} for the phase transition from superconductive to normal nuclear states, Eq. (18), respectively. The experimental excitation spectra were taken from the ENDSF base [55] as in Fig. 1; see the text

Fig. 2 The same as in Fig. 1 but for other nuclei ^{48}Ca, ^{115}Sn, ^{144}Sm, and ^{208}Pb
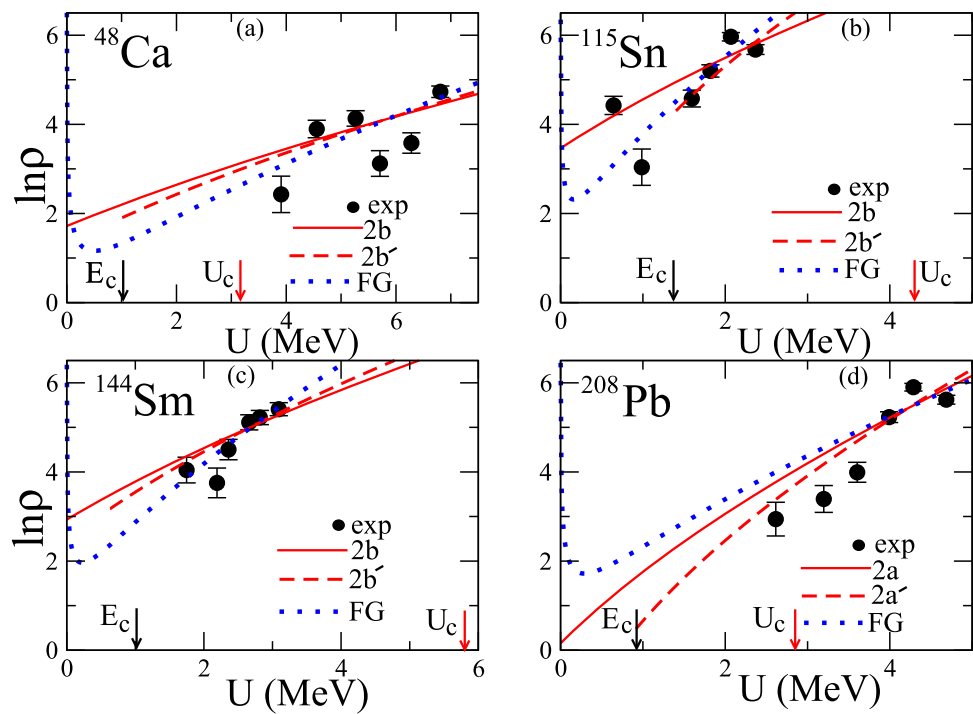

Table 4 The same as in Table 3 but for nuclei ^{48}Ca, ^{115}Sn, ^{144}Sm, and ^{208}Pb, presented in Fig. 2

Nuclei	MMA	$\mathcal{E}_{sh}$	E_{cond} (MeV)	U_c^{tot} (MeV)	K (MeV)	ΔK (MeV)	σ
^{48}Ca	2b′	0.224	1.0	3.2	21.6	1.3	2.6
	2b				23.7	1.2	2.6
	FG				15.5	0.8	2.6
^{115}Sn	2b′	0.061	1.4	4.4	15.6	1.7	3.0
	2b				23.7	1.1	3.1
	FG				11.7	0.6	3.5
^{144}Sm	2b′	0.368	0.6	2.0	34.2	1.2	1.4
	2b				38.8	1.3	1.6
	FG				20.8	0.4	1.1
^{208}Pb	2a′	1.77	0.9	2.9	23.9	0.9	3.2
	2a				28.1	0.9	3.4
	FG				38.3	1.6	3.6

is seen also from a significant difference of the MMA results for the finite condensation energy E_{cond} (dashed lines) and those at $E_{cond} = 0$ (solid lines). An intermediate situation for pairing observation takes place in Fig. 1c, d for a semi-magic ^{54}Fe and non-magic ^{52}Fe; see also Table 3.

In all plots of Fig. 1 and Table 3 we present the dominating shell-structure MMA approach (10) with large ξ^*, especially large for ^{54}Fe [Fig. 1 (c)]. The MMA2a approach [35] with the relative shell-correction energy $\mathcal{E}_{sh}$ from Ref. [53] is associated with the smallest LMSF error σ for calculations in Fig. 1.

Thus, the MMA2a and MMA2a′ results presented in Fig. 1a for ^{40}Ca show a strong shell and pairing effects with

a relatively large shell correction $\mathcal{E}_{sh}$ ($\xi^* \gg 1$), in spite that ^{40}Ca is magic nucleus, in both neutrons and protons; see also Table 3 and Ref. [53]. The pairing energy-condensation contribution [cf. dashed and solid lines in Fig. 1] is significant, especially remarkably seen in Fig. 1a for ^{40}Ca. The pairing shift of the excitation energy notably improves the comparison between the experimental dots and theoretical MMA dashed results. These should be compared with those of the pairing discard version of the MMA approach [MMA2a in (a,d) and MMA2b in (b,c)] shown by solid lines. The pairing effects are smaller in Fig. 1d and, especially, in panels (b, c) than in that of (a).

Figure 2 (Table 4) shows several other situations concerning the pairing contributions. In Fig. 2a we present the same level density as in Fig. 1a but for another double magic isotope ^{48}Ca with a large isotopic asymmetry parameter, $X \approx 0.2$. There is a super-fluidity but essentially below all experimental points as shown by the red arrow. Therefore, the pairing correlations are not easily detected, in contrast to those for ^{40}Ca [Fig. 1a]. The error parameter σ and the value of the inverse level parameter K are significantly higher for ^{48}Ca than in the case of ^{40}Ca. Relatively, the super-fluidity effect measured by the difference between dashed and solid red curves decreases significantly for ^{48}Ca.

The next plot (Fig. 2b) for a semi-magic even-odd nucleus ^{115}Sn is devoted to another exotic case concerning superfluidity. Notice that in this case there are several excitation energies below the condensation energy (two lowest experimental points). This is because there are several lowest nuclear excited states which are significantly below the condensation energy value E_{cond}. These excited states are excluded from our calculations because they give a relatively very small (about 4%) contribution to the total error dispersion σ^2, and almost do not change the result (see Table 4) for σ. Therefore, in this case, almost all experimental points, giving important contributions into the dispersion parameter σ^2, are below the superfluidity-normal phase transition indicated by the red arrow. Thus, one can assume that the even-odd nucleus ^{115}Sn is in principle superfluid in the MMA, as seen also from essential difference of dashed and solid curves. Notice that this approximate MMA result for an even-odd nucleus differs from a more microscopic treatment of pairing in such even-odd nuclei; see, e.g., Ref. [6]. Therefore, we have to clarify more this result by using a modification of the MMA method, e.g., taking into account the Pauli blocking, in our future work, that is beyond the scope of our present work. In contrast to the MMA, within the standard Fermi-gas model, one has negligibly small pairing effects, due to almost zero corresponding change of the background energy in the FG model, in line of Ref. [2].

In the next plot (c) of Fig. 2 for another semi-magic nucleus ^{144}Sm, all experimental points are lying inside of the interval between both arrows for E_c and U_c, that perhaps leads to a good condition for detection of the super-fluidity effects. However, the difference between solid and dashed curves, which is a measure of the superfluity effect, is small in this case, in contrast to the super-fluidity of magic nucleus ^{40}Ca (Fig. 1a) but similar to that for another semi-magic nucleus ^{54}Fe (Fig. 1c).

Much larger difference occurs in the case (d) of Fig. 2 for double magic nucleus ^{208}Pb with about the same asymmetry parameter $X \approx 0.2$ as in the panel (a) of this figure for another double magic nucleus ^{48}Ca (Fig. 2a). But a similar problem for experimental observation of the superfluity effects takes place as in Fig. 2a for ^{48}Ca, and even more similar to those for ^{56}Ni in Fig. 1b. The distance of the pairing collapse energy U_c from the first excitation energy state point is too small in Fig. 2d, almost 300 keV on its right. Therefore, it is difficult to detect the super-fluidity effects in ^{208}Pb. In close similarity with the situation for magic nuclei ^{56}Ni and ^{48}Ca: There is a superfluity transition to the normal state but it is very difficult or even impossible to observe because of a small distance of the pairing collapse energy U_c^{tot}, Eq. (18), to the first excitation energy point.

As shown in Tables 3 and 4, the values of the inverse level density parameter K can be significantly larger than those (about 10 MeV) for the neutron resonances. In all plots of Figs. 1 and 2, one can clearly see also the divergence of the SPM FG lines, Eq. (11), near the zero excitation energy, $U \to 0$. The FG approach has a larger (or sometimes, of the order) value of σ for considered low-energy states in all plots of Figs. 1 and 2, except for that of the semi-magic nucleus ^{144}Sm and magic nucleus ^{48}Ca.

5 Conclusions

We have obtained agreement between the results of the theoretical approximation (MMA) and experimental data [55] for the statistical level density ρ in the low excitation energy states (LES) region for several nuclei with close and open shells and for intermediate situations. Using the mixed micro- and grand-canonical ensembles beyond the standard saddle-point method of the Fermi gas model we take into account the pairing correlations. The derived level density expressions can be approximated by those known as small (combinatoric) and relatively large (Fermi gas) limits with excitation energies U_{eff}, shifted due to pairing correlations. The MMA clearly manifests an advantage over the standard full SPM Fermi gas (FG) approaches at low excitation energies, because the MMA results do not diverge in the limit of small excitation energies. The values of the inverse level density parameter K obtained within the MMA for LES's below neutron resonances in spectra of several super-fluid nuclei are found to be smaller than those obtained at zero condensation energy E_{cond}. The pairing correlation contributions to the MMA significantly improve the agreement with experimental data for magic nuclei as ^{40}Ca.

An existing opinion on the absence of pairing effects in magic (close shell) nuclei as ^{208}Pb and ^{56}Ni can be explained by a very short spectrum length within the superfluid phase transition. Therefore, it might be difficult to detect such effects. As shown for another magic nucleus ^{40}Ca, these critical arguments are basically due to an underestimated role of the statistical averaging for the level density obtained from the excitation states and particle number fluctuations. Another reason is an overestimation of the shell model properties of nuclei in a normal state while we have

a wide superfluid-normal transition beyond the shell model approach. The MMA results were obtained with only one physical LMSF parameter – the inverse level density parameter K. The MMA values of the inverse level density parameter K for LES's can be significantly different from those of the neutron resonances. Simple estimates of pairing condensation contribution in spherical magic nuclei at low excitation energies, sometimes significantly improve the comparison with experimental data.

As perspectives, following ideas of Peter Schuck and his collaborators, (see, e.g., Ref. [21]), it would be nice to extend our results using the super-fluid properties for infinite matter to those for finite nuclei. Another fruitful extension, also in line of activities of Peter Schuck, is applications of our MMA accounting for pairing effects to suitable problems of nuclear astrophysics.

Data availability statement This manuscript has no associated data or the data will not be deposited. [Authors' comment: The calculated values of K were used for the restricted number of nuclei in the specific problem, and do not have a systematic character, and therefore, they are not required to be deposited.]

Appendix A: Semiclassical periodic orbit theory

For the sake of a simple notation, we shall presently restrict ourselves to the case of A nucleons (one kind only) in a given local (HF) potential $V(\mathbf{r})$ as in Refs. [35,48,50–52]. The level density shell corrections can be presented analytically within the periodic orbit theory (POT) in terms of the sum over classical periodic orbits (PO) [48,50,51],

$$\delta g_{\mathrm{scl}}(\varepsilon) = \sum_{\mathrm{PO}} g_{\mathrm{PO}}(\varepsilon),$$
$$g_{\mathrm{PO}}(\varepsilon) = \mathcal{A}_{\mathrm{PO}}(\varepsilon) \cos\left[\frac{1}{\hbar}\mathbb{S}_{\mathrm{PO}}(\varepsilon) - \frac{\pi}{2}\mu_{\mathrm{PO}} - \phi_0\right]. \quad (A1)$$

Here $\mathbb{S}_{\mathrm{PO}}(\varepsilon)$ is the classical action along the PO in the nucleon potential well of the same radius, $R = r_0 A^{1/3}$ ($r_0 \approx 1.14$ fm), μ_{PO} is the so called Maslov index, determined by the catastrophe points (turning and caustic points) along the PO, and ϕ_0 is an additional shift of the phase coming from the dimension of the problem and degeneracy of the POs. The amplitude $\mathcal{A}_{\mathrm{PO}}(\varepsilon)$, and the action $\mathbb{S}_{\mathrm{PO}}(\varepsilon)$, are smooth functions of the energy ε. In addition, the amplitude, $\mathcal{A}_{\mathrm{PO}}(\varepsilon)$, depends on the PO stability factors. The Gaussian local aver-

aging of the level density shell correction, $\delta g_{\mathrm{scl}}(\varepsilon)$, over the single-particle (s.p.) energy spectrum ε_i near the Fermi surface ε_F, with a width parameter γ, smaller than a distance between major shells, $\mathcal{D}_{\mathrm{sh}}$, can be done analytically [48,50,51],

$$\delta g_{\gamma\,\mathrm{scl}}(\varepsilon) \cong \sum_{\mathrm{PO}} g_{\mathrm{PO}}(\varepsilon)\, \exp\left[-\left(\frac{\gamma t_{\mathrm{PO}}}{2\hbar}\right)^2\right], \quad (A2)$$

where $t_{\mathrm{PO}} = \partial\mathbb{S}_{\mathrm{PO}}/\partial\varepsilon$ is the period of particle motion along the PO in the potential well.

The smooth ground-state energy of the nucleus is approximated by $\tilde{E} \approx E_{\mathrm{ETF}} = \int_0^{\tilde{\lambda}} \mathrm{d}\varepsilon\, \varepsilon\, \tilde{g}(\varepsilon)$, where $\tilde{g}(\varepsilon)$ is a smooth level density equal approximately to the ETF level density, $\tilde{g} \approx g_{\mathrm{ETF}}$, ($\lambda \approx \tilde{\lambda}$, and $\tilde{\lambda}$ is the smooth chemical potential in the SCM). The chemical potential λ (or $\tilde{\lambda}$) is the solution of the corresponding conservation of particle number equation:

$$A = \int_0^\lambda \mathrm{d}\varepsilon\, g(\varepsilon)\,. \quad (A3)$$

The POT shell component of the free energy, δF_{scl}, is related in the non-thermal and non-rotational limit to the shell correction energy of a cold nucleus, δE_{scl}, see Refs. [48,50, 51]. Within the POT, δE_{scl} is determined, in turn, by the oscillating level density $\delta g_{\mathrm{scl}}(\varepsilon)$, Eq. (A1),

$$\delta E_{\mathrm{scl}} \approx \sum_{\mathrm{PO}} \frac{\hbar^2}{t_{\mathrm{PO}}^2} \delta g_{\mathrm{PO}}(\lambda)\,. \quad (A4)$$

The chemical potential λ can be approximated by the Fermi energy ε_F, up to a small excitation energy, and isotopic asymmetry corrections ($T \ll \lambda$ for the saddle point value $T = 1/\beta^*$, if exists). It is determined by the particle-number conservation conditions, Eq. (A3), where $g(\varepsilon) \cong g_{\mathrm{scl}} = g_{\mathrm{ETF}} + \delta g_{\mathrm{scl}}$ is the total POT level density. One now needs to solve equation (A3) to determine the chemical potential λ as function of the particle number A since λ is needed in Eq. (A4) to obtain the semiclassical energy shell correction δE_{scl}.

For a major shell structure near the Fermi energy surface $\varepsilon \approx \lambda$, the POT energy shell correction, δE_{scl}, is approximately proportional to the level density shell correction, $\delta g_{\mathrm{scl}}(\varepsilon)$ [Eq. (A1)], at $\varepsilon = \lambda$, Eq. (A4),

$$\delta E \approx \delta E_{\mathrm{scl}} \approx \left(\frac{\mathcal{D}_{\mathrm{sh}}}{2\pi}\right)^2 \delta g_{\mathrm{scl}}(\lambda)\,, \quad (A5)$$

where $\mathcal{D}_{\mathrm{sh}} \approx \lambda/A^{1/3}$ is the mean distance between major nuclear shells. Indeed, the rapid convergence of the PO sum in Eq. (A4) is guaranteed by the factor in front of the density component g_{PO}, Eq. (A1), a factor which is inversely proportional to the period time $t_{\mathrm{PO}}(\lambda)$ squared along the PO. Therefore, only POs with short periods which occupy a significant phase-space volume near the Fermi surface will contribute.

These orbits are responsible for the major shell structure, that is related to a Gaussian averaging width, $\gamma \approx \gamma_{\text{sh}}$, which is much larger than the distance between neighboring s.p. states but much smaller than the distance $\mathcal{D}_{\text{sh}}$ between major shells near the Fermi surface. Eq. (A2) for the averaged s.p. level density was derived under these conditions for γ. According to the POT [48,50,51], the distance between major shells, $\mathcal{D}_{\text{sh}}$, is determined by a mean period of the shortest and most degenerate POs, $\langle t_{\text{PO}} \rangle$ [50]:

$$\mathcal{D}_{\text{sh}} \cong \frac{2\pi\hbar}{\langle t_{\text{PO}} \rangle} \approx \frac{\lambda}{A^{1/3}} \ . \tag{A6}$$

Taking the factor in front of g_{PO}, in Eq. (A4) off the sum over the POs for the energy shell correction δE_{scl}, one arrives at its semiclassical expression (A5) [48,49,51]. Differentiating Eq. (A5) with (A1) with respect to λ and keeping only the dominating terms coming from differentiation of the sine of the action phase argument, $\mathbb{S}_{\text{PO}}/\hbar \sim A^{1/3}$, one finds the useful relationships:

$$\frac{\partial^2 \delta E_{\text{PO}}}{\partial \lambda^2} \approx -\delta g_{\text{PO}}(\lambda) \ ,$$
$$\frac{\partial^2 g_{\text{scl}}}{\partial \lambda^2} \approx \sum_{\text{PO}} \frac{\partial^2 \delta g_{\text{PO}}}{\partial \lambda^2} \approx -\left(\frac{2\pi}{D_{\text{sh}}}\right)^2 \delta g_{\text{PO}}(\lambda) \ . \tag{A7}$$

Notice that taking into account Eq. (A3) for the chemical potential λ, one has another useful relationship for the second derivative of background thermodynamic potential, $\Omega_0 = \int_0^\lambda \mathrm{d}\varepsilon (\varepsilon - \lambda) g_{\text{scl}}(\varepsilon)$:

$$\frac{\partial^2 \Omega_0}{\partial \lambda^2} \approx -g_{\text{scl}}(\lambda) \ . \tag{A8}$$

The level density parameter a [see Eq. (10) for the entropy S] can be related to the averaged POT level density ETF and shell correction components by

$$a \approx a_{\text{ETF}} + \delta a_{\text{scl}} = \frac{\pi^2}{6}(g_{\text{ETF}} + \delta g_{\text{scl}}) \ , \tag{A9}$$

For shell corrections, one has the following relation:

$$\delta a_{\text{scl}} = \frac{\pi^2}{6} \delta g_{\text{scl}}(\lambda). \tag{A10}$$

Using Eqs. (A9), (A10), and Eq. (A7), one obtains Eq. (9).

References

1. T. Ericson, Adv. Phys. **9**, 425 (1960)
2. A.A. Bohr, B.R. Mottelson, *Nuclear Structure*, vol. 1 (Benjamin, New York, 1967)
3. L.D. Landau, E.M. Lifshitz, *Statistical Physics, Course of Theoretical Physics*, vol. 5 (Pergamon, Oxford, 1975)
4. A.V. Ignatyuk, *Statistical Properties of Excited Atomic Nuclei* (Energoatomizdat, 1983). (**Russian**)
5. N.K. Grossjean, H. Feldmeier, Nucl. Phys. A **444**, 113 (1985)
6. Yu.V. Sokolov, *Level Density of Atomic Nuclei* (Energoatomizadat, 1990). (**Russian**)
7. S. Shlomo, Nucl. Phys. A **539**, 17 (1992)
8. A.V. Ignatyuk, Level densities, in *Handbook for Calculations of Nuclear Reaction Data*. (International Atomic Energy Agency, Vienna, 1998), pp.65–80
9. Y. Alhassid, G.F. Bertsch, L. Fang, Phys. Rev. C **68**, 044322 (2003)
10. T. von Egidy, D. Bucurescu, Phys. Rev. C **78**, 051301(R) (2008)
11. T. von Egidy, D. Bucurescu, Phys. Rev. C **80**, 054310 (2009)
12. Y. Alhassid, G.F. Bertsch, C.N. Gilbreth, H. Nakada, Phys. Rev. C **93**, 044320 (2016)
13. V.M. Kolomietz, A.I. Sanzhur, S. Shlomo, Phys. Rev. C **97**, 064302 (2018)
14. V. Zelevinsky, A. Volya, *Mesoscopic Nuclear Physics: From Nucleus To Quantum Chaos To Quantum Signal* (World Scientific, Singapore, 2018)
15. V. Zelevinsky, M. Horoi, Prog. Part. Nucl. Phys. **105**, 180 (2019)
16. V.M. Kolomietz, S. Shlomo, *Mean Field Theory* (World Scientific, Cham, 2020)
17. R. Bengtsson, P. Schuck, Phys. Lett. B **89**, 321 (1980)
18. P. Ring, P. Schuck, *The Nuclear Many-Body Problem* (Springer-Verlag, New York, 1980)
19. J.L. Egido, P. Ring, S. Iwasaki, H.J. Mang, Phys. Lett. B **154**, 1 (1985)
20. H. Kucharek, P. Ring, P. Schuck, R. Bengtsson, M. Girod, Phys. Lett. B **216**, 249 (1989)
21. H. Kucharek, P. Ring, P. Schuck, Z. Phys. A **334**, 119 (1989)
22. M. Farine, P. Schuck, X. Viñas, Phys. Rev. A **62**, 013608 (2000)
23. X. Viñas, P. Schuck, M. Farine, M. Centelles, Phys. Rev. C **67**, 054314 (2003)
24. M. Baldo, C. Maieron, P. Schuck, X. Viñas, Nucl. Phys. A **736**, 241 (2004)
25. F. Barranco, P.F. Bortignon, R.A. Broglia, G. Colo, P. Schuck, E. Vigezzi, X. Viñas, Phys. Rev. C **72**, 054314 (2005)
26. X. Viñas, P. Schuck, M. Farine, arXiv:1010.5961v1 [nucl.phys] (2010)
27. X. Viñas, P. Schuck, M. Farine, J. Phys: Conf. Ser. **321**, 012024 (2011)
28. A. Pastore, J. Margueron, P. Schuck, X. Viñas, Phys. Rev. C **88**, 034314 (2013)
29. P. Schuck, X. Viñas, *Fifty Years of Nuclear BCS* (World Scientific, 2013), pp.212–226
30. A. Pastore, P. Schuck, X. Viñas, J. Margueron, Phys. Rev. A **90**, 043634 (2014)
31. A. Pastore, P. Schuck, X. Viñas, arXiv:2004.09423 [nucl-th] (2020)
32. P. Schuck, M. Urban, X. Viñas, Eur. Phys. J. A **59**, 164 (2023)
33. A.I. Levon et al., Phys. Rev. C **102**, 014308 (2020)
34. V.M. Kolomietz, A.G. Magner, V.M. Strutinsky, Sov. J. Nucl. Phys. **29**, 758 (1979)
35. A.G. Magner, A.I. Sanzhur, S.N. Fedotkin, A.I. Levon, S. Shlomo, Int. J. Mod. Phys. E **30**, 2150092 (2021)
36. A.G. Magner, A.I. Sanzhur, S.N. Fedotkin, A.I. Levon, S. Shlomo, Phys. Rev. C **104**, 044319 (2021)
37. A.G. Magner, A.I. Sanzhur, S.N. Fedotkin, A.I. Levon, S. Shlomo, Nucl. Phys. A **1021**, 122423 (2022)
38. A.G. Magner, A.I. Sanzhur, S.N. Fedotkin, A.I. Levon, U.V. Grygoriev, S. Shlomo, Low Temp. Phys. **48**, 920 (2022)
39. A.G. Magner, A.I. Sanzhur, S.N. Fedotkin, A.I. Levon, U.V. Grygoriev, S. Shlomo, Nucl. Phys. At. Energy **24**, 175 (2023)
40. M. Brack, L. Damgaard, A.S. Jensen, H.C. Pauli, V.M. Strutinsky, C.Y. Wong, Rev. Mod. Phys. **44**, 320 (1972)
41. V.M. Strutinsky, On the nuclear level density in case of an energy gap, in *Proceedings of the International Conference on Nuclear Physics*. (Springer, 1958), pp.617–622
42. A. Bohr, B.R. Mottelson, D. Pines, Phys. Rev. **110**, 936 (1958)
43. S.T. Belyaev, Mat. Fys. Medd. Dan. Vid. Selsk **31**, 3 (1959)
44. J. Bardeen, L.N. Cooper, J.R. Schrieffer, Phys. Rev. **108**, 1175 (1957)

45. L.D. Landau, E.M. Lifshitz, *Statistical Physics, Part 2, Course of Theoretical Physics*, vol. 9 (Pergamon, London, 1980)
46. A. Sedrakian, J.W. Clark, Eur. Phys. J. A **55**, 167 (2019)
47. B. Le Crom et al., Phys. Lett. B **829**, 137057 (2022)
48. V.M. Strutinsky, A.G. Magner, Sov. J. Part. Nucl. **7**, 138 (1976)
49. V.M. Strutinsky, A.G. Magner, S.R. Ofengenden, T. Døssing, Z. Phys. A **283**, 269 (1977)
50. M. Brack, R.K. Bhaduri, *Semiclassical Physics Frontiers in Physics, No. 96*, vol. 2 (Westview Press, Boulder, 2003)
51. A.G. Magner, Y.S. Yatsyshyn, K. Arita, M. Brack, Phys. At. Nucl. **74**, 1445 (2011)
52. M. Brack, C. Guet, H.-B. Håkansson, Phys. Rep. **123**, 275 (1985)
53. P. Moeller, A.J. Sierk, T. Ichikawa, H. Sagawa, At. Data Nucl. Data Tables **109–110**, 1–204 (2016)
54. P. Vogel, B. Jonson, P.G. Hansen, Phys. Lett. **139**, 227 (1984)
55. National Nuclear Data Center On-Line Data Service for the ENSDF database, http://www.nndc.bnl.gov/ensdf